High-Efficiency Ternary Nonfullerene Organic Solar Cells with a Record Long-Term Thermal Stability

Cai'e Zhang,[a] Shouli Ming,[a] Hongbo Wu,[b] Xiaodong Wang,[a] Hao Huang,[a] Wenyue Xue,[c] Xinjun Xu,[a*] Zheng Tang,[b*] Wei Ma,[c*] Zhishan Bo[a*]

[a] Key Laboratory of Energy Conversion and Storage Materials, College of Chemistry, Beijing Normal University, Beijing 100875, China.

[b] Center for Advanced Low-dimension Materials, State Key Laboratory for Modification of Chemical Fibers and Polymer Materials, College of Materials Science and Engineering, Donghua University, Shanghai 201620, China.

[c] State Key Laboratory for Mechanical Behavior of Materials, Xi'an Jiaotong University, Xi'an 710049, China.

*Corresponding authors. E-mail: xuxj@bnu.edu.cn (X.X.), ztang@dhu.edu.cn (Z.T.), msewma@mail.xjtu.edu.cn (W.M.), zsbo@bnu.edu.cn (Z.B.)

Cai'e Zhang and Shouli Ming contributed equally to this work.

1.1 Materials and Instruments

Unless otherwise noted, all chemicals were purchased from commercial suppliers and used without further purification. IDT-PDOT-C6 (2,2'-((2Z,2'Z)-((8,8'-(4,4,9,9-tetrakis(4-hexylphenyl)-4,9-dihydro-s-indaceno[1,2-b:5,6-b']dithiophene-2,7-diyl)bis(3,3-dihexyl-3,4-dihydro-2H-thieno[3,4-b][1,4]dioxepine-8,6-diyl))bis(methanylylidene))bis(5,6-difluoro-3-oxo-2,3-dihydro-1H-indene-2,1-diylidene))dimalononitrile) was synthesized according to our previous work. ITC6-IC and ITC6-4F were synthesized according to the reported procedure.[1,2] The catalyst precursor $Pd(PPh_3)_4$ was prepared according to the literature, and stored in a Schlenk tube under nitrogen atmosphere. Unless otherwise noted, all reactions were performed under an atmosphere of nitrogen and monitored by thin layer chromatography (TLC)

on silica gel. Column chromatography was carried out on silica gel (200–300 mesh). ^{1}H and ^{13}C NMR spectra were recorded on a Bruker AV 400 spectrometer. UV-visible absorption spectra were obtained on a PerkinElmer UV-vis spectrometer (Model Lambda 750). Mass spectrometry (MS) (MALDI-TOF) results were performed with an Autoflex III instrument. The absolute fluorescence quantum yields were tested with Edinburgh FLS980 Spectrometer under the Xenon source light path and NIRPMT-sphere detector light path.

Thermal gravimetric analysis (TGA) and differential scanning calorimetry (DSC) measurements were performed on TA2100 and Perkin-Elmer Diamond DSC instrument, respectively, under a nitrogen atmosphere at a heating rate of 10 ^{o}C/min. Atomic force microscopy (AFM) measurements were performed under ambient conditions using a Digital Instrument Multimode Nanoscope IIIA operating in the tapping mode. Transmission electron microscopy (TEM, Tecnai F20, FEI) was operated at an accelerating voltage of 200 kV. The thickness of the blend films was determined by a Dektak 6 M surface profile meter. The powder X-ray diffraction (XRD) patterns were collected using a PANalytical X'Pert PRO MPD diffractometer with Cu Kα radiation. Grazing Incidence Wide-Angle X-ray Scattering (GIWAXS) measurements were performed at beamline 7.3.3 at the Advanced Light Source. Samples were prepared on Si substrates using identical blend solutions as those used in devices. The 10 keV X-ray beam was incident at a grazing angle of 0.12°-0.16°, selected to maximize the scattering intensity from the samples. The scattered x-rays were detected using a Dectris Pilatus 2M photon counting detector. The electrochemical behavior of the polymers was investigated using cyclic voltammetry (CHI 630A Electrochemical Analyzer) with a standard three-electrode electrochemical cell in a 0.1 M Bu_4NPF_6 solution in CH_3CN at room temperature under an atmosphere of nitrogen with a scanning rate of 0.1 V/s. A Pt plate working electrode, a Pt wire counter electrode, and an $Ag/AgNO_3$ (0.01M in CH_3CN) reference electrode were used. The experiments were calibrated with the standard ferrocene/ferrocenium (Fc/Fc^{+}) redox system and assumption that the energy level of Fc is 4.8 eV below vacuum.

Synthesis of *ITC6-2F*

Compound **1** was prepared in satisfactory yields according to previously reported procedures.[1] To a solution of compound **1** (150 mg, 0.12 mmol) and compound **2** (purchased from Solarmer Materials Inc.) (254 mg, 1.20 mmol) in $CHCl_3$ (50 ml) was added pyridine (1 ml) under nitrogen atmosphere. The mixture was refluxed for 16 h and then cooled to room temperature. After evaporation of the solvent under vacuum, the residue was purified by column chromatography on silica gel, yielding 141 mg of ITC6-IC-2F as a duck blue solid (Yield: 72%). ^{1}H NMR (400 MHz, $CDCl_3$): δ 9.03 (d, 2H), 8.69 (dd, 1H), 8.36 (d, 1H), 7.88 (m, 1H), 7.62 (d, 2H), 7.53 (d, 1H), 7.39 (m, 2H), 7.21 (d, 8H), 7.13 (d, 8H), 3.11 (t, 4H), 2.55 (t, 8H), 1.76 (m, 4H), 1.57 (m, 8H), 1.34 (m, 4H), 1.28 (m, 32H), 0.84 (m, 18H); ^{13}C NMR (100 MHz, $CDCl_3$): δ 186.88, 167.66, 167.25, 165.61, 165.18, 155.72, 152.84, 152.38, 147.93, 145.45, 142.52, 142.36, 142.28, 140.03, 138.97, 136.92, 135.85, 134.86, 133.11, 128.85, 127.90, 127.72, 125.72, 125.65, 122.10, 121.92, 118.60, 115.22, 115.07, 114.55, 112.82, 112.62, 110.73, 110.55, 68.92, 68.01, 63.39, 35.62, 31.83, 31.71, 31.26, 30.85, 29.75, 29.20, 22.60, 22.46, 14.0.9, 13.93.

1.2 Solar Cells Fabrication and Characterization

OSCs were fabricated with the device configuration of ITO/ZnO/active layer/MoO_3 /Ag through the following steps. The indium tin oxide (ITO) glass was precleaned sequentially in an ultrasonic bath of water, acetone, isopropanol and water, each for 20 min. The substrates were dried on a hotplate at 160 ^{o}C for 10 min, which were then treated with UV-ozone for 25 min. The ZnO precursor was prepared by dissolving zinc acetate dehydrate (Aldrich, 99.9%, 1 g) and ethanolamine (Aldrich, 99.5%, 0.28 g) in 2-methoxyethanol (Aldrich, 99.8%, 10 mL) under vigorous stirring for over 8 h for the hydrolysis reaction. A thin layer of ZnO was spin-coated on top of the precleaned ITO substrates at 3500 rpm for 20 s and annealed at 200 ^{o}C for 20 min on a hot-plate before

being transferred into a glove box. The binary and ternary blend films keep the same optimal donor/receptor weight ratio of 1:1 (the two acceptors were mixed with different ratios to fabricate the ternary OSCs) with a polymer concentration of 4 mg mL^{-1} in the 1,2-dichlorobenzene solution (without any additives), and then spin-coated at 1500 rpm for 50 s to obtain a film thickness of 110 nm on the top of the ITO/ZnO layer after thermal annealing 160 ^{o}C for 5 min. An 8.5 nm MnO_3 layer and 100 nm Ag layer were subsequently evaporated onto the active layer, at a vacuum pressure below 10^{-7} Torr. Photovoltaic cells were fabricated on the substrate with an effective area of 0.04 cm^2. The *J-V* curves of photocurrents were recorded in glove box at approximately 25 °C using an instrument from Enli Technology Ltd., Taiwan (SS-F53A) under AM 1.5G illumination (AAA class solar simulator, with an intensity of 100 mW cm^{-2} calibrated with a standard single crystal Si photovoltaic cell). The thermal stability of optimized solar cells, kept under continuous heating at 75 °C in the glove box. External quantum efficiency (EQE) measurements were conducted in air without encapsulation. The EQE data were obtained using a solar cell spectral response measurement system (QER3011, Enli Tech-nology Co. Ltd), and the intensity was calibrated with a standard single-crystal Si photovoltaic cell.

Space-Charge-Limited-Current Measurement

Hole and electron-only devices with a structure of ITO/PEDOT:PSS/active layer/Au and ITO/ZnO/active layer/Al were fabricated, respectively. A solution of PBDB-T and acceptors in 1,2-dichlorobenzene (DCB) was spin-coated onto PEDOT:PSS or ZnO to form the active layer, then Au (or Al) was thermally evaporated at a pressure of 10^{-4} Pa through a shadow mask. Dark *J-V* curves of the hole/electron-only devices were measured and charge mobilities were calculated by the space-charge-limited-current (SCLC) method.[10.1103/PhysRevB.58.R13411, 10.1063/1.1891301] Dark *J-V* curves were fitted by using the Mott-Gurney equation: $J = 9\varepsilon_o\varepsilon_r\mu V/8d^3$, where J is the space charge limited current, ε_0 is the vacuum permittivity ($\varepsilon_o = 8.85\times10^{-12}$ F/m), ε_r is the permittivity of the active layer ($\varepsilon_r \approx 3$), μ is charge mobility, and d is the thickness of the active

layer.

Determination of Flory–Huggins interaction parameter (χ)

The surface energy γ values could be calculated according to the Wu model on the neat films by Equations 1 and 2:[3]

$$\gamma = \gamma^d + \gamma^p \quad (1)$$

$$\gamma_{LV}(1+\cos\theta) = \frac{4\gamma_S^d\gamma_L^d}{\gamma_S^d+\gamma_L^d} + \frac{4\gamma_S^p\gamma_L^p}{\gamma_S^p+\gamma_L^P} \quad (2)$$

And the two different contact angles of water and glycerol are measured to achieve the γ of acceptor and polymer donor, and the results are shown in Supplementary Table S10. And the γ is the sum of dispersion (d) and polar (p) components.

As $\delta \propto \sqrt{\gamma}$, we could calculate all the solubility parameter (δ) of acceptor and polymer.[4] Further, the Flory-Huggins interaction parameter χ could be calculated according to the Equation 3:[4]

$$\chi_{ij} = \frac{V_1}{RT}(\delta_1 - \delta_2)^2 + 0.34 \quad (3)$$

Since we adopt the *o*-DCB as the solvent, the V_1 is 113.3 $cm^3\ mol^{-1}$. We calculate the χ of the blend of small molecular acceptors and PBDB-T, and the results are shown in Table 3.

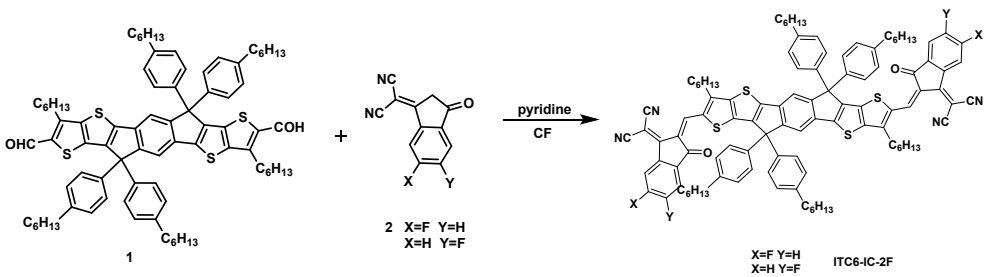

Scheme S1. The synthetic route for ITC6-2F.

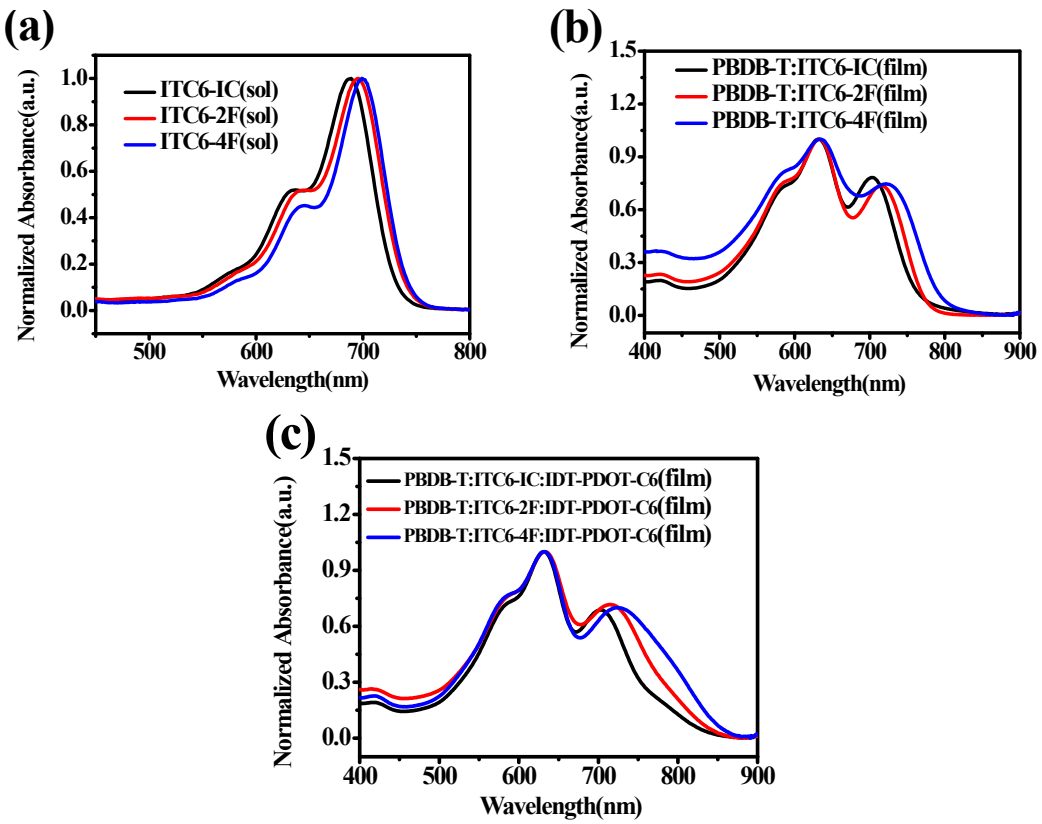

Fig. S1 UV-vis absorption spectra of acceptors in solutions (a) and in binary (b) or ternary (c) blend films.

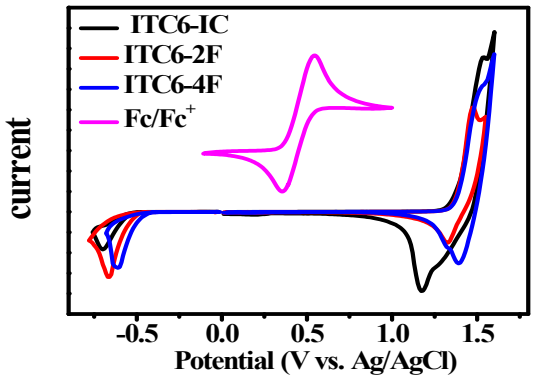

Fig. S2 Cyclic voltammogram of ITC6-IC, ITC6-2F and ITC6-4F measured in acetonitrile solutions using ferrocene (Fc/Fc^{+}) as an internal standard.

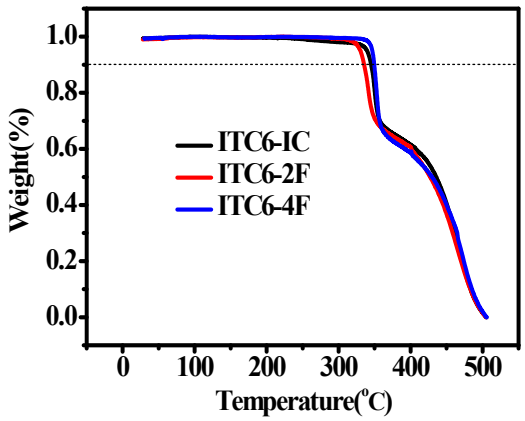

Fig. S3 TGA curves of ITC6-IC, ITC6-2F and ITC6-4F under nitrogen atmosphere.

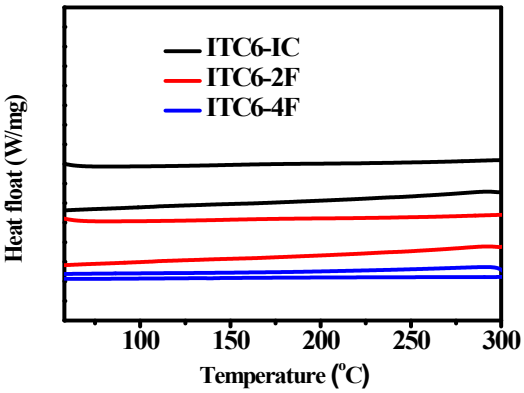

Fig. S4 DSC curves of ITC6-IC, ITC6-2F and ITC6-4F under nitrogen atmosphere.

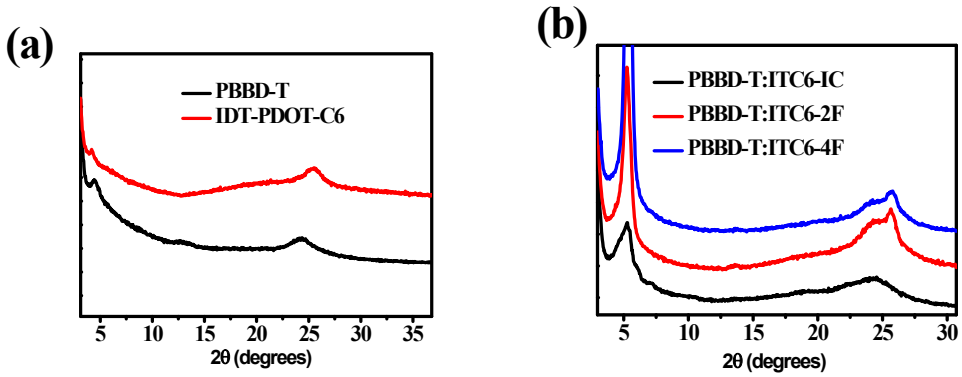

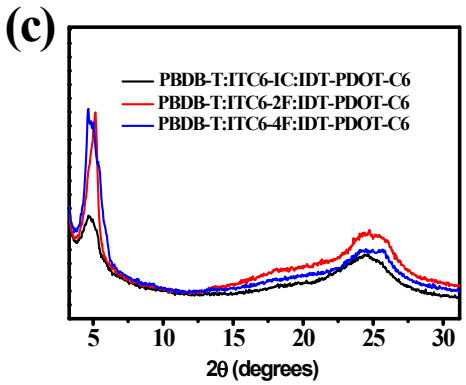

Fig. S5 XRD patterns of (a) PBDB-T and IDT-PDOT-C6 neat films, (b) binary blend films of PBDB-T:ITC6-IC/ITC6-2F/ITC6-4F, and (c) ternary blend films of PBDB-T:ITC6-IC/ITC6-2F/ITC6-4F:IDT-PDOT-C6.

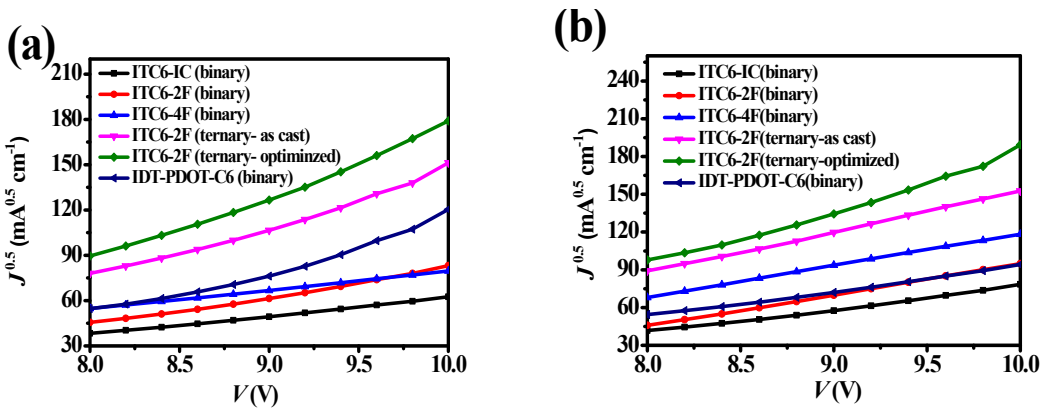

Fig. **S6** *J-V* curves for the (a) hole mobility and (b) electron mobility measurements of ITC6-IC, ITC6-2F, ITC6-4F, and IDT-PDOT-C6 based binary and ternary devices.

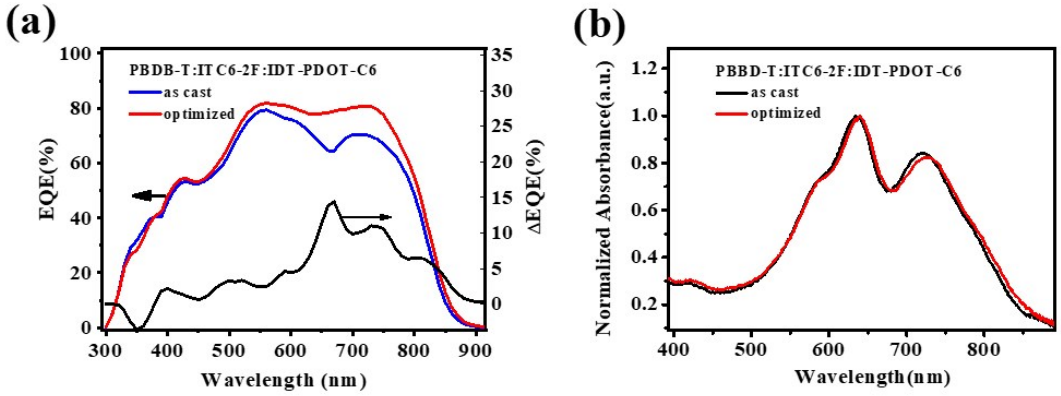

Fig. S7 EQE (a) and UV-vis absorption (b) spectra of the as cast and optimized ternary PBDB-T:ITC6-2F:IDT-PDOT-C6. Inset in a) shows the difference spectrum of EQE between the as-cast and optimized ternary blend devices.

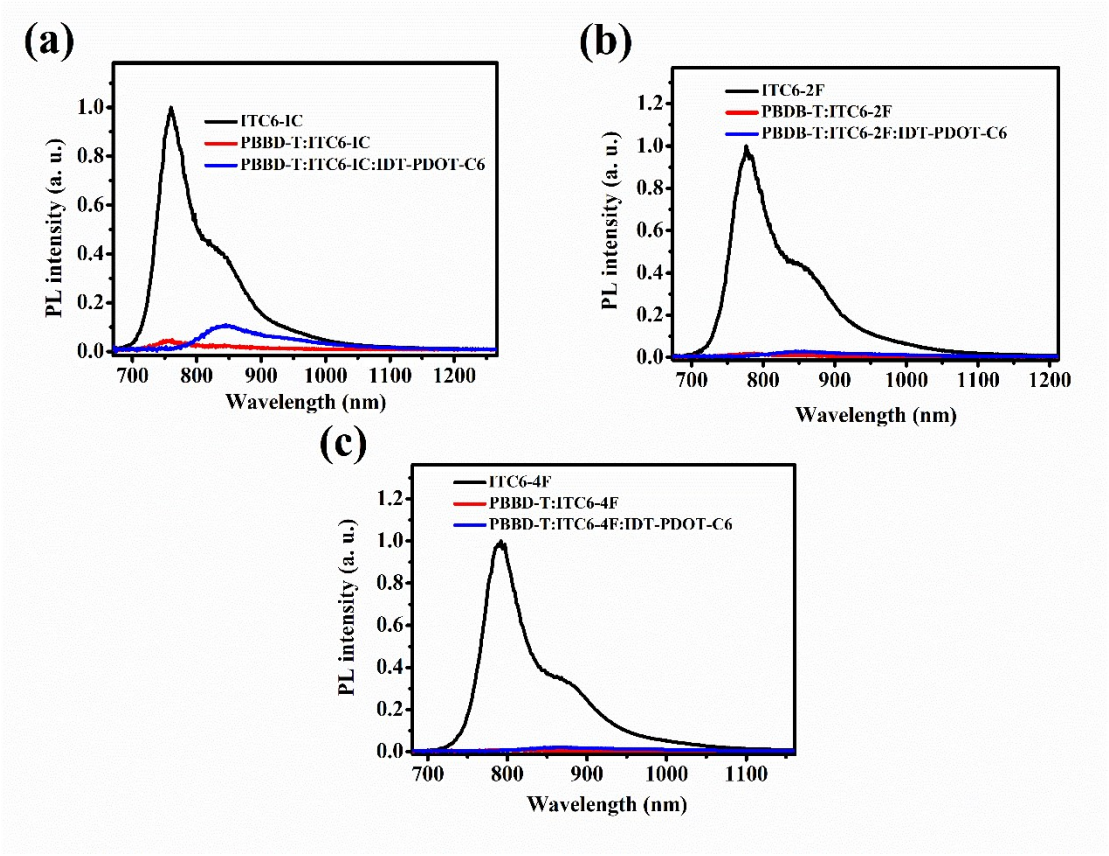

Fig. S8 Photoluminescence spectra of neat acceptor (excitated at 650 nm) and the binary and ternary blend films (excitated at 650 nm): (a) ITC6-IC, (b) ITC6-2F, and (c) ITC6-4F.

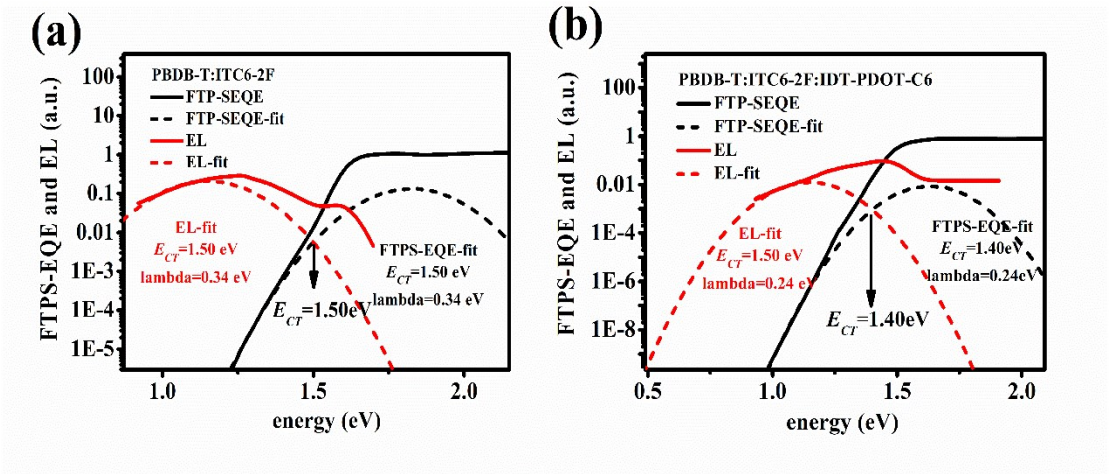

Fig. S9 Determination of the E_{CT} values for PBDB-T:ITC6-2F (a) and PBDB-T:ITC6-2F:IDT-PDOT-C6 (b) blends from the corresponding reduced FTPS-EQE (solid black lines) and EL (solid red lines) spectra. The dashed black and red curves are the fit results.

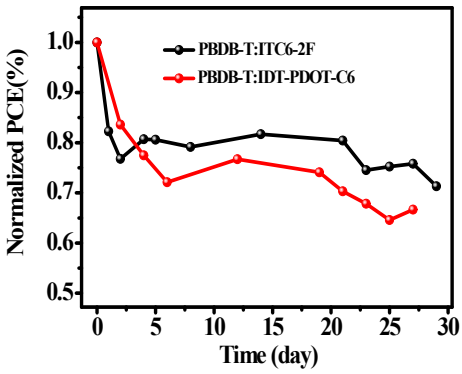

Fig. S10 PCE stability tests of the binary PBDB-T:ITC6-2F and PBDB-T:IDT-PDOT-C6 devices in the dark at 75 °C.

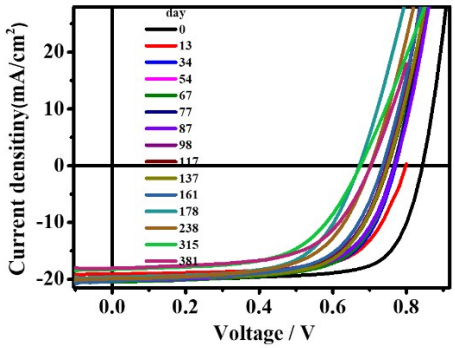

Fig. S11 original *J-V* data of device stability.

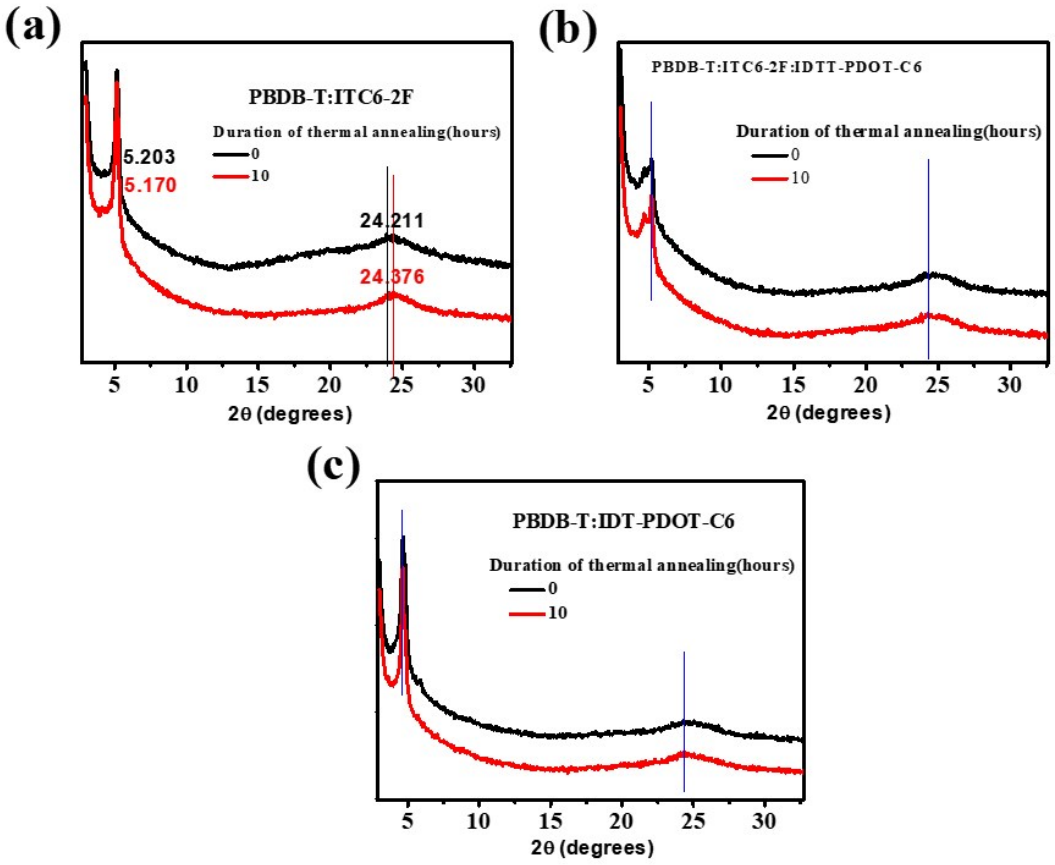

Fig. S12 XRD patterns of (a) PBDB-T:ITC6-2F, (b) PBDB-T:ITC6-2F:IDT-PDOT-C6, and (c) PBDB-T:IDT-PDOT-C6 blend films without thermal annealing and 10-hours annealing at 75 °C in air.

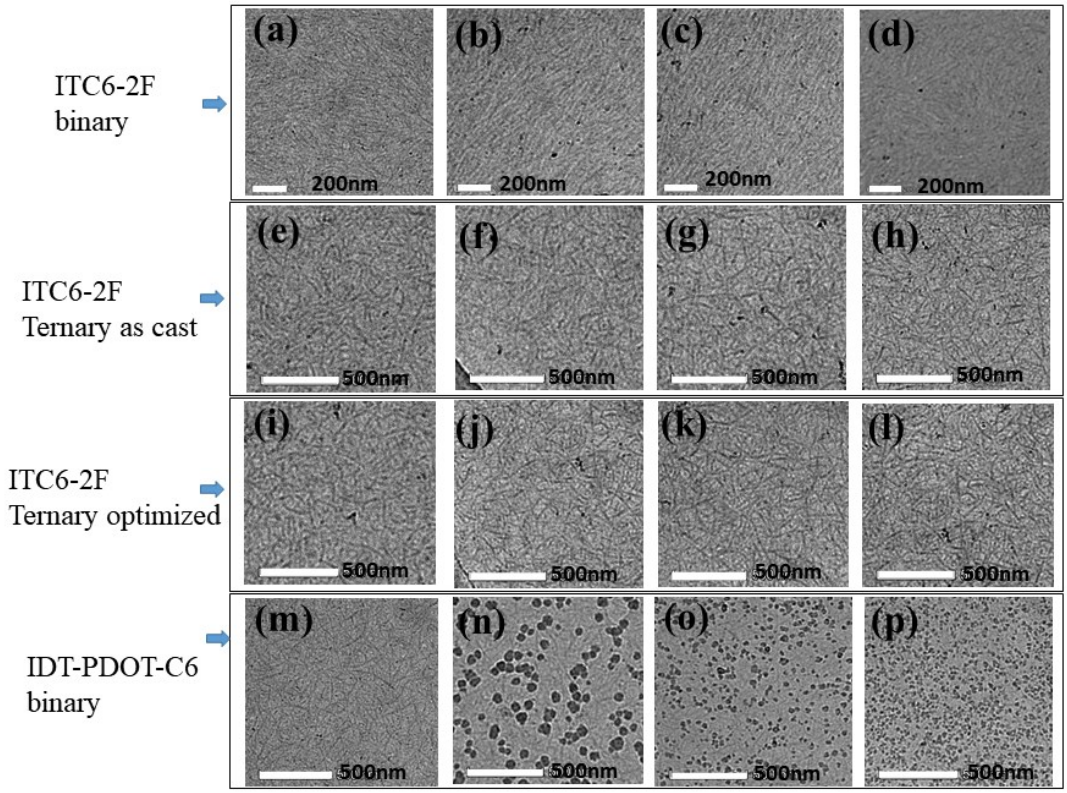

Fig.S13 TEM images of PBDB-T:ITC6-2F a)-d), PBDB-T:ITC6-2F:IDT-PDOT-C6 as cast e)-h), PBDB-T:ITC6-2F:IDT-PDOT-C6 optimized i)-l), and PBDB-T:IDT-PDOT-C6 m-p) blend films under continuous heating for 0, 10, 48, and 72 hours, respectively, at 75 °C in air.

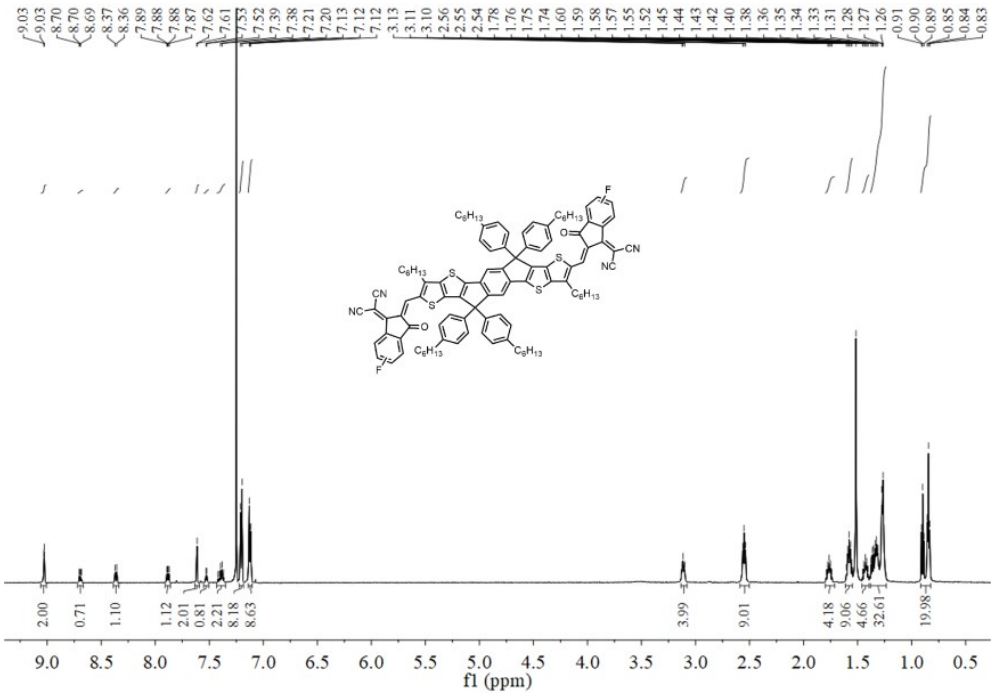

Fig. S14 ^{1}H NMR of ITC6-2F in $CDCl_3$.

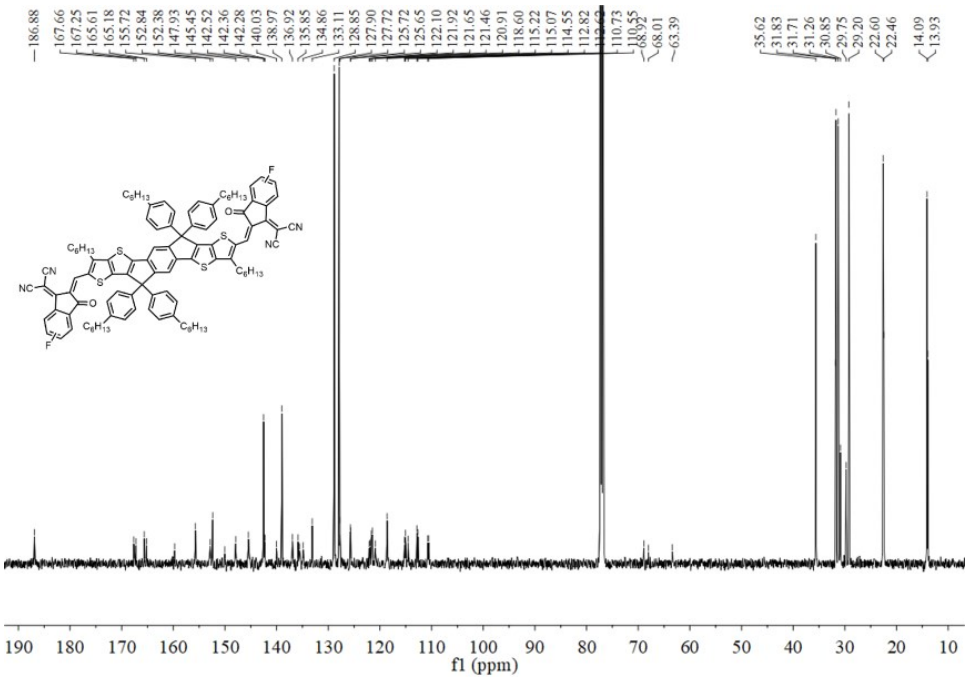

Fig. S15 ^{13}C NMR of ITC6-2F in $CDCl_3$.

Table S1 Parameters derived from XRD patterns of neat films.

Film	2θ (°)	lamellar distance (Å)	2θ (°)	π-π stackingdistance (Å)
ITC6-IC	5.11	17.28	22.98	3.87
ITC6-2F	5.13	17.24	23.70	3.75
ITC6-4F	5.42	16.30	25.36	3.51
IDT-PDOT-C6	4.18	21.12	25.45	3.50
PBDB-T	4.45	19.86	24.22	3.67

Table S2 Hole and electron mobilities of OSCs.

Active layer	**μ_e [$cm^2 V^{-1}s^{-1}$]**	**μ_h [$cm^2 V^{-1}s^{-1}$]**	**μ_e/μ_h**

(weight ratios)			
PBDB-T:ITC6-IC (1:1)	6.56×10^{-5}	1.51×10^{-4}	0.43
PBDB-T:ITC6-2F (1:1)	1.58×10^{-4}	2.74×10^{-4}	0.58
PBDB-T:ITC6-4F (1:1)	2.68×10^{-4}	2.85×10^{-4}	0.94
PBDB-T:ITC6-2F:IDT-PDOT-C6 (1:0.6:0.4) as cast	5.66×10^{-4}	4.64×10^{-4}	1.21
PBDB-T:IDT-PDOT-C6 (1:1)	4.57×10^{-4}	1.79×10^{-4}	2.55
PBDB-T:ITC6-2F:IDT-PDOT-C6 (1:0.6:0.4) optimized	8.81×10^{-4}	8.98×10^{-4}	0.98

Table S3 Photovoltaic parameters of ITC6-2F based ternary devices with different contents (weight ratio) in the acceptor.

PBDB-T:ITC6-2F:IDT-PDOT-C6	V_{oc} (V)	J_{sc} (mA/cm^2)	FF (%)	PCE (%)
1:1:0	0.861	17.83	72.80	11.20
1:0.8:0.2	0.879	19.75	67.11	11.66
1:0.6:0.4	0.883	19.84	69.83	12.23
1:0.4:0.6	0.900	19.81	65.20	11.58
1:0.2:0.8	0.900	19.55	64.62	11.35
1:0:1	0.903	18.94	62.25	10.67

Table S4. Photovoltaic parameters of PBDB-T:ITC6-2F:IDT-PDOT-C6 (1:0.6:0.4) based devices after treatment under various annealing temperatures.

PBDB-T:ITC6-2F:IDT-PDOT-C6	$T_{annealing}$ (°C)	V_{oc} (V)	J_{sc} (mA/cm^2)	FF (%)	PCE (%)
	r.t.	0.883	19.84	69.83	12.23
	80	0.885	19.89	68.43	12.05
	100	0.878	19.98	68.46	12.01

1:0.6:0.4	120	0.874	19.99	69.20	12.09
	140	0.876	20.17	70.64	12.48
	160	0.853	21.73	72.06	13.36
	180	0.804	22.15	67.65	12.10

Table S5 Photovoltaic parameters of ITC6-IC based ternary devices with different contents (weight ratio) in the acceptor.

PBDB-T:ITC6-IC:IDT-PDOT-C6	V_{oc} (V)	J_{sc} (mA/cm^2)	FF (%)	PCE (%)
1:1:0	0.938	16.24	71.15	10.87
1:0.8:0.2	0.934	17.95	65.59	11.03
1:0.6:0.4	0.932	18.49	65.65	11.34
1:0.4:0.6	0.920	18.61	65.84	11.30
1:0.2:0.8	0.916	19.62	62.58	11.28
1:0:1	0.903	19.01	61.70	10.60

Table S6 Photovoltaic parameters of PBDB-T:ITC6-IC:IDT-PDOT-C6 (1:0.4:0.6) based devices after treatment under various annealing temperatures.

PBDB-T:ITC6-IC:IDT-PDOT-C6	*Annealing* (°C)	V_{oc} (V)	J_{sc} (mA/cm^2)	FF (%)	PCE (%)
1:0.6:0.4	r.t.	0.931	18.49	65.65	11.34
	80	0.914	18.80	64.29	11.05
	100	0.926	18.73	68.34	11.85
	120	0.927	19.02	68.40	12.06
	140	0.920	18.49	68.21	12.13
	160	0.9.5	18.73	69.66	12.30
	180	0.920	18.80	70.41	12.23

Table S7 Photovoltaic parameters of ITC6-4F based ternary devices with different contents (weight ratio) in the acceptor.

PBDB-T:ITC6-4F:IDT-PDOT-C6	V_{oc} (V)	J_{sc} (mA/cm^2)	FF (%)	PCE (%)
1:1:0	0.776	18.55	73.18	10.48
1:0.8:0.2	0.786	19.34	70.15	10.61
1:0.6:0.4	0.809	20.66	67.10	11.17
1:0.4:0.6	0.858	20.02	66.70	11.40
1:0.2:0.8	0.867	19.81	63.31	10.82
1:0:1	0.903	18.94	62.25	10.67

Table S8 Photovoltaic parameters of PBDB-T:ITC6-4F:IDT-PDOT-C6 (1:0.4:0.6) based devices after treatment under various annealing temperatures.

PBDB-T:ITC6-4F:IDT-PDOT-C6	Annealing (°C)	V_{oc} (V)	J_{sc} (mA/cm^2)	FF (%)	PCE (%)
1:0.4:0.6	r.t.	0.858	20.02	66.70	11.40
	120	0.851	20.35	64.11	11.05
	140	0.843	20.71	64.12	11.15
	160	0.849	20.85	68.32	12.04
	180	0.844	20.89	68.49	12.02
	200	0.831	21.46	65.85	11.68

Table S9 Coherence lengths of the (100) and (010) peaks and the *d*-spacings for the pristine PBDB-T, the binary blended (PBDB-T:ITC6-IC/ITC6-2F/ITC6-4F/IDT-PDOT-C6) and ternary blended (PBDB-T:ITC6-2F:IDT-PDOT-C6) films.

	Lamellar	**π–π** stacking distance (010)

Active Layer	distance (100)			
	$dl^{a)}$[Å] [q_{xy}(Å^{-1})]	$d_{\pi}^{b)}$[Å] [q_z(Å^{-1})]	FWHM $^{c)}$ (Å^{-1})	CCL$^{d)}$ (Å)
PBDB-T:ITC6-IC	21.57 (0.291)	3.75 (1.68)	0.29	19.58
PBDB-T:ITC6-2F	21.56 (0.291)	3.74 (1.68)	0.29	19.54
PBDB-T:ITC6-4F	21.66 (0.290)	3.74 (1.68)	0.28	20.35
PBDB-T:IDT-PDOT-C6	21.73 (0.289)	3.64 (1.73)	0.26	21.47
PBDB-T:ITC6-2F:IDT-PDOT-C6	21.49 (0.292) 18.66(0.337)	3.65 (1.72)	0.23	24.59

[a)](100) diffraction peak along the q_{xy} axis; [b)](010) diffraction peak along the q_z axis; [c)]Full width at half-maximum (FWHM) for the (010) peak along the q_z axis; [d)]Coherence length estimated from the Scherrer's equation (CCL = 2πk/FWHM) for the π–π stacking of the face-on crystallite.

Table S10 Contact angle (θ) of water and glycerol and surface tension (γ) of ITC6-2F, IDT-PDOT-C6 and PBDB-T.

Materials	θ_{water} [°]	$\theta_{glycerol}$ [°]	γ [mJ/m]
ITC6-2F	102.3	90.1	20.90
IDT-PDOT-C6	105.5	96.6	18.06
PBDB-T	104.1	90.6	22.00

References

1. Z. Zhang, J. Yu, X. Yin, Z. Hu, Y. Jiang, J. Sun, J. Zhou, F. Zhang, T. Russell, F. Liu, W. Tang, *Adv. Funct. Mater.,* 2018, **28**,1705095.

2. Z. Zhang, X. Liu, J. Yu, H. Wang, M. Zhang, L. Yang, R. Geng, J. Cao, F. Du, F. Liu and W. Tang, *J. Mater. Chem. C,* 2019, **7**, 13279-13286.

3. Comyn J. *Int. J. Adhes. Adhes.,* 1992, **12**, 145-149.

4. S. Nilsson, S. Nilsson, A Bernasik, A Budkowski, E. Moons. Macromolecules*.,* 2007, **40**, 8291-8301.

5. S. Li, L. Zhan, F. Liu, J. Ren, M. Shi, C. Z. Li, T. P. Russell and H. Chen, *Adv. Mater.,* 2018, **30,**1705208.

6. H. Hu, L. Ye, M. Ghasemi, N. Balar, J. J. Rech, S. J. Stuard, W. You, B. T. O'Connor and H. Ade, *Adv. Mater.,* 2019, **31**, e1808279.

7. Y. Dong, Y. Zou, J. Yuan, H. Yang, Y. Wu, C. Cui and Y. Li, *Adv. Mater.,* 2019, 1904601.

8. Z. Liu and N. Wang, *Adv.Opt. Mater.*, 2019, 1901241.

9. Y. Wang, W. Lan, N. Li, Z. Lan, Z. Li, J. Jia and F. Zhu, *Adv. Energy Mater.*, 2019, **9**, 1900157.

10. H. Liu, Z. X. Liu, S. Wang, J. Huang, H. Ju, Q. Chen, J. Yu, H. Chen and C. Z. Li, *Adv. Energy Mater.,* 2019, **9**, 1900887.

11. Y. Xu, J. Yuan, S. Liang, J.-D. Chen, Y. Xia, B. W. Larson, Y. Wang, G. M. Su, Y. Zhang, C. Cui, M. Wang, H. Zhao and W. Ma, *ACS Energy Lett*, 2019, **4**, 2277-2286.

12. Y. Gong, K. Chang, C. Chen, M. Han, X. Zhan, J. Min, X. Jiao, Q. Li and Z. Li, *Mat Chem Front*, 2019, **3**, 93-102.

13. J. Guo, H. Bin, W. Wang, B. Chen, J. Guo, R. Sun, Z.-G. Zhang, X. Jiao, Y. Li and J. Min, *J. Mater. Chem. A,* 2018, **6**, 15675-15683.

14. S. Oh, C. E. Song, T. Lee, A. Cho, H. K. Lee, J.-C. Lee, S.-J. Moon, E. Lim, S. K. Lee and W. S. Shin, *J. Mater. Chem. A,* 2019, **7**, 22044-22053.

15. Y. Xin, G. Zeng, J. OuYang, X. Zhao and X. Yang,*J. Mater. Chem. C,* 2019, **7**, 9513-9522.

16. H. Chen, Z. Hu, H. Wang, L. Liu, P. Chao, J. Qu, W. Chen, A. Liu and F. He, *Joule,* 2018, **2**, 1623-1634.

17. P. Cheng, C. Yan, Y. Wu, J. Wang, M. Qin, Q. An, J. Cao, L. Huo, F. Zhang, L. Ding, Y. Sun, W. Ma and X. Zhan, *Adv. mater,* 2016, **28**, 8021-8028.

18. X. Song, N. Gasparini, M. M. Nahid, S. H. K. Paleti, J.-L. Wang, H. Ade and D. Baran, *Joule,* 2019, **3**, 846-857.

19. G. E. Park, S. Choi, S. Y. Park, D. H. Lee, M. J. Cho and D. H. Choi, *Adv. Energy Mater*, 2017, **7**, 1700566.

20. X. Du, Y. Yuan, L. Zhou, H. Lin, C. Zheng, J. Luo, Z. Chen, S. Tao and L.-S. Liao, *Adv. Fun.Mater.*, 2020, 1909837.